Perfect separation of intraband and interband excitations in $PdCoO_2$

C. C. Homes,[1,*] S. Khim,[2] and A. P. Mackenzie[2,3,†]

[1]*Condensed Matter Physics and Materials Science Division, Brookhaven National Laboratory, Upton, New York 11973, USA*

[2]*Max Planck Institute for Chemical Physics of Solids, Nöthnitzer Strasse 40, 01187 Dresden, Germany*

[3]*Scottish Universities Physics Alliance, School of Physics & Astronomy, University of St. Andrews, North Haugh, St. Andrews KY16 9SS, United Kingdom*

(Received 2 November 2018; revised manuscript received 20 March 2019; published 15 May 2019)

The temperature dependence of the optical properties of the delafossite $PdCoO_2$ has been measured in the *a-b* planes over a wide frequency range. The optical conductivity due to the free-carrier (intraband) response falls well below the interband transitions, allowing the plasma frequency to be determined from the *f*-sum rule. Drude-Lorentz fits to the complex optical conductivity yield estimates for the free-carrier plasma frequency and scattering rate. The in-plane plasma frequency has also been calculated using density functional theory. The experimentally determined and calculated values for the plasma frequencies are all in good agreement; however, at low temperature the optically determined scattering rate is much larger than the estimate for the transport scattering rate, indicating a strong frequency-dependent renormalization of the optical scattering rate. In addition to the expected in-plane infrared-active modes, two very strong features are observed that are attributed to the coupling of the in-plane carriers to the out-of-plane longitudinal optic modes.

DOI: 10.1103/PhysRevB.99.195127

I. INTRODUCTION

The delafossite $PdCoO_2$ is one of only a handful of transition metal oxides whose in-plane resistivity at room temperature rivals that of silver or copper ($\simeq 2\ \mu\Omega\,\mathrm{cm}$), establishing a new benchmark for conducting metal oxides [1]. Perhaps even more remarkable is the large residual resistivity ratio (RRR $\gtrsim 400$) and extremely low in-plane residual resistivity at low temperature $\rho_{ab} \simeq 8\ \mathrm{n}\Omega\,\mathrm{cm}$ [2,3], which may place this material in the hydrodynamic limit [4,5]. Given the quasi-two-dimensional (2D) behavior of this material [2], it is inevitable to compare it with the 2D cuprate materials, perhaps the most studied of the conducting metal oxides. The cuprates are typically described as bad metals [6] in which the resistivity often shows a peculiar nonsaturating linear temperature dependence that may violate the Mott-Ioffe-Regel limit at high temperature [7,8]; the optical conductivity reveals an unusual free-carrier response where the scattering rate is strongly renormalized with frequency, resulting in an incoherent response that merges with other bound excitations [9]. Surprisingly, in both of these materials the free carriers originate from a single band at the Fermi level. The common structural motif in the cuprates is the square copper-oxygen plaquettes where the conducting states originate; however, $PdCoO_2$ is different in that it crystalizes in the trigonal $R\bar{3}m$ (166) space group, consisting of Pd triangular layers and CoO_2 triangular slabs [1], shown in the inset of Fig. 1. There is theoretical [10–13] as well as experimental [14] evidence that the density of states at the Fermi level is dominated by Pd rather than Co, indicating that the conduction originates in the Pd layers. The exceptionally long in-plane mean free paths of $\simeq 20\ \mu\mathrm{m}$ at low temperature implies that the Pd layers are almost completely free of any disorder, since the mean free path corresponds to $\simeq 10^5$ lattice spacings [15], a situation that is difficult to justify given that the crystals are grown using flux-based techniques.

In this work the complex optical properties of $PdCoO_2$ have been determined for light polarized in the *a-b* planes over a wide frequency range at a variety of temperatures. The real part of the optical conductivity reveals that the free-carrier response is completely isolated from the interband transitions, allowing the plasma frequency to be determined from the *f*-sum rule. The free-carrier response has also been fit using the Drude-Lorentz model, returning values for the plasma frequency and scattering rate. In addition, the in-plane and out-of-plane plasma frequencies and interband optical conductivities have been calculated using density functional theory. The calculated and experimentally determined plasma frequencies are all in good agreement. However, at low temperature the experimentally determined optical scattering rate is much larger than the estimated transport scattering rate; this disagreement may only be resolved if the optical scattering rate is assumed to vary quadratically with frequency (Fermi liquid), as opposed to the linear dependence observed in the cuprates (marginal Fermi liquid). Finally, in addition to the expected in-plane infrared-active modes, two very strong features are observed that are attributed to the coupling of the in-plane carriers with the out-of-plane longitudinal optic (LO) modes [16], indicating the presence of electron-phonon coupling.

II. EXPERIMENT

Single crystals of $PdCoO_2$ were grown in an evacuated quartz ampoule with a mixture of $PdCl_2$ and CoO as described

*homes@bnl.gov
†andy.mackenzie@cpfs.mpg.de

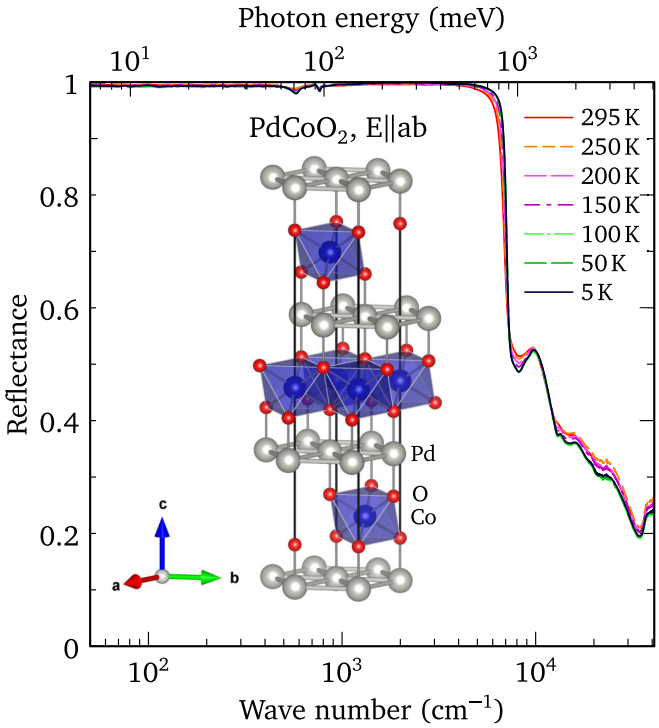

FIG. 1. The temperature dependence of the reflectance of $PdCoO_2$ for light polarized in the *a-b* planes showing its extremely high value over the far- and mid-infrared regions until a sharp plasma edge is encountered at $\simeq$6000 cm^{-1}. Inset: The unit cell of $PdCoO_2$ depicting the triangular coordination of the Pd atoms and the CoO_2 slabs within the *a-b* planes [22].

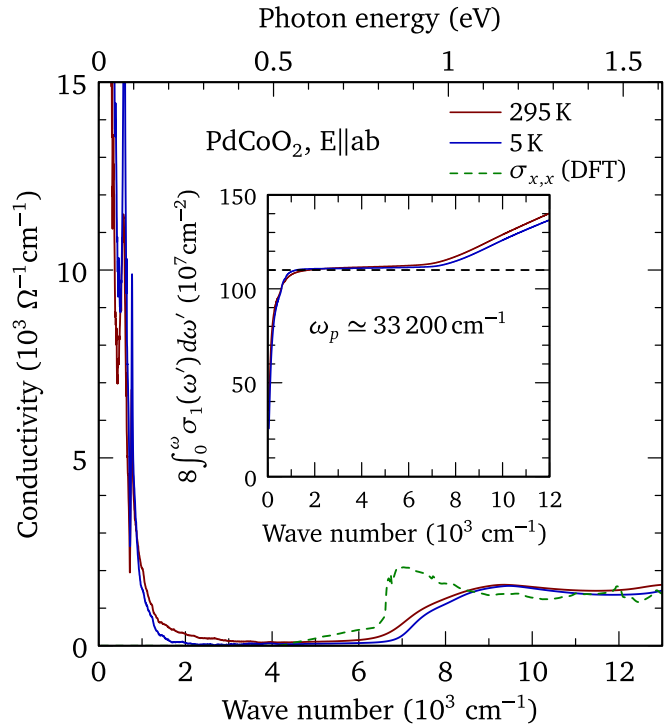

FIG. 2. The real part of the optical conductivity of $PdCoO_2$ for light polarized in the *a-b* planes at 295 and 5 K showing the complete separation of the low-frequency intraband excitations below $\simeq$1500 cm^{-1}, and the interband transitions, which have an onset at $\simeq$7000 cm^{-1}. The calculated optical conductivity due to the interband transitions is denoted by $\sigma_{x,x}$. Inset: The spectral weight associated with the conductivity sum rule at 295 and 5 K.

in Refs. [1,17], yielding thin platelets of typical dimensions 1 mm $\times$ 1 mm $\times$ 100 μm. The reflectance of $PdCoO_2$ was measured at a near-normal angle of incidence for light polarized in the *a-b* planes at a variety of temperatures over a wide frequency range ($\simeq$5 meV to 5 eV) using an overfilling and *in situ* evaporation technique [18]. While the reflectance contains a great deal of information, it is a combination of the real and imaginary parts of the refractive index, and as such it is not an intuitive quantity. The complex optical properties have been calculated from a Kramers-Kronig analysis of the reflectance [19,20], which requires extrapolations for $\omega \rightarrow 0, \infty$. Below the lowest-measured frequency point, a Hagen-Rubens form is employed, $R(\omega) \propto 1 - a\sqrt{\omega}$, where a is chosen to match the data. Above the highest-measured frequency, the reflectance is assumed to have the power-law dependence $R(\omega) \propto 1/\omega$ up to 1.5×10^5 cm^{-1}, above which a free-electron $1/\omega^4$ behavior is assumed.

III. RESULTS AND DISCUSSION

The temperature dependence of the reflectance is shown over a wide frequency range in Fig. 1; a remarkable feature of the reflectance is its extremely high value ($\gtrsim$0.99) over the far- and mid-infrared regions, with a sharp plasma edge at $\simeq$6000 cm^{-1} ($\simeq$0.7 eV). We note that this measurement is particularly challenging because at room temperature the in-plane reflectance of $PdCoO_2$ in this region is already higher than that of gold or silver [21], two elements that are used as optical references. Despite the dramatic decrease in the resistivity at low temperature [3], the only noticeable change in the reflectance is a slight sharpening of the plasma edge. Interestingly, there is also structure in the 500–800 cm^{-1} region, the energy range associated with lattice vibrations.

A. Complex conductivity

The real part of the optical conductivity is shown over a wide spectral region at 295 and $\simeq$5 K in Fig. 2. Interestingly, at low temperature the low-frequency conductivity associated with the free-carrier response is limited to below $\simeq$1500 cm^{-1}; as a consequence, there is no overlap with the interband transitions which are observed above $\simeq$7000 cm^{-1}. The *f*-sum rule allows that in the absence of other excitations $\int_0^\omega \sigma_1(\omega')d\omega' = \omega_p^2/8$, where $\omega_p^2 = 4\pi ne^2/m^*$ is the square of plasma frequency with carrier concentration n and effective mass m^*, and the cut-off frequency ω is chosen so that ω_p converges smoothly (here σ_1 has the units of cm^{-1}). The inset in Fig. 2 shows the result of this conductivity sum rule up to $\sim$1.5 eV; the integral has converged by about $\omega \simeq 1000\,cm^{-1}$, yielding a value of $\omega_p \simeq 33\,200 \pm 600$ cm^{-1} at both 295 and 5 K; this is close to the value of $\omega_p \simeq 38\,200$ cm^{-1} determined from a de Haas–van Alphen study [3].

The optical conductivity may also be fit to the Drude-Lorentz model with the complex dielectric function

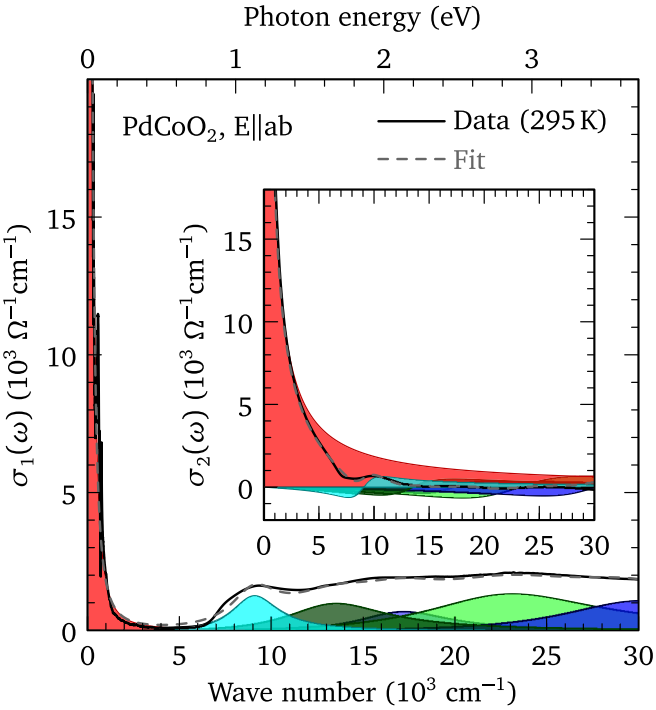

FIG. 3. The real part of the optical conductivity of $PdCoO_2$ at 295 K for light polarized in the *a-b* planes (solid line), compared to the fit to the Drude-Lorentz model (dashed line), which is decomposed into the individual Drude and Lorentz oscillator components; the overall quality of the fit is quite good (see Table I for parameter values). Inset: The imaginary part of the optical conductivity (solid line), compared to the fitted value (dashed line). Compared to the real part, the free-carrier response of the imaginary part is considerably broader.

$$\tilde{\epsilon} = \epsilon_1 + i\epsilon_2,$$

$$\tilde{\epsilon}(\omega) = \epsilon_\infty - \frac{\omega_p^2}{\omega^2 + i\omega/\tau_{\rm op}} + \sum_j \frac{\Omega_j^2}{\omega_j^2 - \omega^2 - i\omega\gamma_j}, \quad (1)$$

where ϵ_∞ is the real part of the dielectric function at high frequency, ω_p is previously defined, and $1/\tau_{\rm op}$ is the scattering rate for the delocalized (Drude) carriers; typically, $1/\tau_{\rm op}$ is nearly identical to the scattering rate determined from transport measurements, $1/\tau_{\rm tr}$. In the summation, ω_j, γ_j, and Ω_j are the position, width, and strength of the jth transverse optic (TO) mode or a bound excitation, respectively. The complex conductivity is $\tilde{\sigma} = \sigma_1 + i\sigma_2 = 2\pi i\omega[\epsilon_\infty - \tilde{\epsilon}(\omega)]/Z_0$ (in units of $\Omega^{-1}\,{\rm cm}^{-1}$), where $Z_0 = 377\ \Omega$ is the impedance of free space. The results of the simultaneous fit to the real and imaginary parts of the optical conductivity of $PdCoO_2$ at 295 K for light polarized in the *a-b* planes with a single Drude component and five Lorentz oscillators using a nonlinear least-squares technique is shown in Fig. 3; the values of the fitted parameters are listed in Table I. The fit to the real part of the optical conductivity returns a Drude component with $\omega_p \simeq 33\,300\ {\rm cm}^{-1}$ and $1/\tau_{\rm op} \simeq 97\ {\rm cm}^{-1}$. While the result for the plasma frequency is in excellent agreement with the value determined from the *f*-sum rule, the value for $1/\tau_{\rm op}$ is more than an order of magnitude smaller than the scattering rate suggested from photoemission experiments

TABLE I. The Drude-Lorentz model parameters fitted to the real and imaginary parts of the optical conductivity of $PdCoO_2$ at 295 K for light polarized in the *a-b* planes. All values are in units of ${\rm cm}^{-1}$, unless otherwise indicated.[a]

Component	j	ω_j	$1/\tau_{op}$, γ_j	ω_p, Ω_j
Drude		–	97	33 317
Lorentz	1	9099	3067	15 200
Lorentz	2	13 555	6620	19 760
Lorentz	3	17 223	6085	15 880
Lorentz	4	23 135	11 585	30 360
Lorentz	5	30 200	10 557	26 190

[a]$\epsilon_\infty = 3.4$.

[14]. The corresponding fit to the imaginary part of the optical conductivity in the inset of Fig. 3 indicates that the free-carrier response extends well into the mid-infrared region and allows the high-frequency part of the dielectric function to be determined, $\epsilon_\infty \simeq 3.4$. A minimal number of oscillators has been used to describe the relatively flat optical conductivity at high frequency; however, it should be noted that the placement of the high-frequency mode (ω_5) is somewhat arbitrary.

B. Scattering rates

Using the Drude expression for the dc conductivity $\sigma_0 \equiv \sigma_1(\omega \to 0) = 2\pi\omega_p^2\tau_{\rm op}/Z_0$ with the values for the fitted parameters at 295 K yields $\sigma_0 \simeq 1.85 \times 10^5\ \Omega^{-1}\,{\rm cm}^{-1}$, or in terms of the resistivity, $\rho_0 \simeq 5.4\ \mu\Omega\,{\rm cm}$, which is close to the transport value $\rho_{\rm dc} \simeq 2.6\ \mu\Omega\,{\rm cm}$ [3]. Given that $\rho_{ab}(300\ {\rm K})/\rho_{ab}(2\ {\rm K}) \simeq 400$ [23], and $\rho_{\rm dc} \propto 1/\tau_{\rm tr}$, then at low temperature $1/\tau_{\rm tr} \lesssim 0.3\ {\rm cm}^{-1}$; however, fits to both the optical conductivity and the plasma edge in the reflectance at $\simeq$5 K yield the significantly larger values of $1/\tau_{\rm op} \simeq 80 \pm 10\ {\rm cm}^{-1}$. While a value for $1/\tau_{\rm op} \lesssim 1\ {\rm cm}^{-1}$ might reasonably be thought to result in a plasma edge in the reflectance that resembles a step function, the proximity to nearby interband transitions has the effect of significantly broadening this feature.

To demonstrate this effect, the reflectance $R = \tilde{r}\tilde{r}^*$ has been calculated at a normal angle of incidence; $\tilde{r} = (\tilde{n} - 1)/(\tilde{n} + 1)$ is the Fresnel reflectance, which is related to the dielectric function through the complex refractive index $\tilde{\epsilon} = \tilde{n}^2 = (n + ik)^2$. The Drude reflectance is initially calculated in the absence of any interband excitations for $\omega_p = 33\,500\ {\rm cm}^{-1}$ with a scattering rate of $1/\tau_{\rm op} = 1\ {\rm cm}^{-1}$, and $\epsilon_\infty = 25$ (the value of ϵ_∞ is chosen to place the renormalized plasma frequency $\omega_p/\sqrt{\epsilon_\infty}$ close to the experimentally observed position); the resulting plasma edge is extremely sharp with a sharp drop at just over 0.8 eV that resembles a step function, shown by the dashed line in Fig. 4.

The five interband excitations in Table I have been added to the reflectance; however, the low-frequency oscillator is described by $\omega_1 = 9100\ {\rm cm}^{-1}$, with width $\gamma_1 = 3100\ {\rm cm}^{-1}$, and a gradually increasing value of the oscillator strength of $\Omega_1 = 0 \to 15\,000\ {\rm cm}^{-1}$ (the values of ϵ_∞ have been adjusted by hand to keep the value of the reflectance at high frequency roughly constant); the addition of the interband terms, the low-frequency oscillator in particular, has the effect of broadening

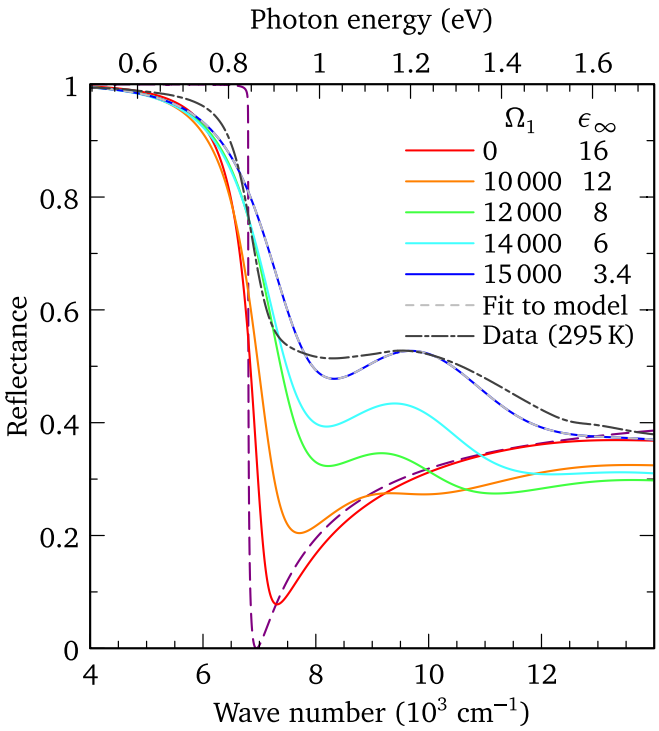

FIG. 4. The experimentally determined reflectance of $PdCoO_2$ for light polarized in the *a*-*b* planes at 295 K (dash-dot line), compared to the calculated reflectance for free carriers with $\omega_p = 33\,500$ cm^{-1}, $1/\tau_{op} = 1$ cm^{-1}, and $\epsilon_\infty = 25$ in the absence of any other excitations (dashed line), and in the presence of an interband transition with $\omega_1 = 9100$ cm^{-1}, $\gamma_1 = 3100$ cm^{-1}, and varying strengths $\Omega_1 = 0 \rightarrow 15\,000$ cm^{-1} ($\epsilon_\infty = 16 \rightarrow 3.4$), along with four other high-frequency modes (Table I). The Drude-Lorentz fit to the upper reflectance curve reproduces the model perfectly (Table II).

the Drude plasma edge considerably, as well as shifting the minima to higher frequency. The broadened nature of the plasma edge in the reflectance might make it difficult to determine the intrinsic value of the free-carrier scattering rate.

To test this possibility, we have fit the upper curve in Fig. 4 that most closely resembles the experimental reflectance at 295 K (dash-dot line) using the model values in Table II (the remaining high-frequency oscillators are taken from Table I), employing a spectral resolution of 8 cm^{-1} (less than or equal to the experimental resolution in the mid- and near-infrared regions). The free-carrier component and the low-frequency oscillator are fit to the reflectance using a nonlinear least-squares method, while the four high-frequency modes are kept fixed; the fitted results are identical to the model values, which are summarized in Table II. This indicates that despite the broadening of the plasma edge in the reflectance due to nearby interband transitions, as well as an instrumental resolution that is lower than the intrinsic width of this feature, the values for $1/\tau_{op} \lesssim 1$ cm^{-1} may still be accurately determined from fits to the reflectance (or complex conductivity).

TABLE II. Initial parameters for the Drude-Lorentz model, as well as the seed and final values for the fit to the model reflectance.[a] The high-frequency oscillators used in the model, ω_2 through ω_5 (Table I) are kept fixed. All units are in cm^{-1}.

Parameter	Model value	Seed value	Fitted value
ω_p	33 500	30 000	33 500
$1/\tau_{op}$	1.0	100	1.00
ω_1	9100	9000	9100
γ_1	3100	2000	3100
Ω_1	15 000	10 000	15 000

[a]The model value is $\epsilon_\infty = 3.4$; the seed value is 5, the fitted value is 3.4.

Thus, we conclude that there is a profound disagreement between the optical and transport scattering rates at low temperature, $1/\tau_{op} \gg 1/\tau_{tr}$. This discrepancy may arise if within a single band the optical scattering rate is strongly renormalized with frequency, as described by the generalized Drude model [24,25]

$$1/\tau_{op}(\omega) = \frac{2\pi\omega_p^2}{Z_0}\,\mathrm{Re}\left[\frac{1}{\tilde{\sigma}(\omega)}\right]. \tag{2}$$

However, this approach is complicated by the fact that $\sigma_1(\omega) \propto 1/[1 - R(\omega)]$; because the reflectance is close to unity, even a small uncertainty can result in large changes to σ_1, and subsequently the scattering rate, making the experimentally determined values unreliable.

While the in-plane transport at very low temperatures is rather unusual and perhaps governed by phonon-drag effects [3], in general this material may be regarded as a Fermi liquid [2], where the scattering rate is quadratic in both temperature and frequency, $1/\tau(\omega, T) = 1/\tau_0 + a(\hbar\omega)^2 + b(k_B T)^2$, where $b/a = \pi^2$ [24]. In the $\omega \rightarrow 0$ (dc) limit $1/\tau(T) = 1/\tau_0 + b(k_B T)^2$, with a residual scattering rate $1/\tau_0 \simeq 0.14$ cm^{-1} [3]. Using the Drude scattering rate $1/\tau_{op} \simeq 100$ cm^{-1} at 295 K we can estimate $b \simeq 2.383 \times 10^{-3}$ cm [26]. In the frequency domain at low temperature, $1/\tau_{op}$ is then the average of $1/\tau(\omega)$ over the interval $0 \rightarrow \omega$,

$$1/\tau_{op} = \frac{1}{\omega}\int_0^\omega 1/\tau(\omega')\,d\omega' \simeq \frac{b}{3\pi^2}\omega^2. \tag{3}$$

From Fig. 2 a reasonable estimate for ω would be the point at which most of the spectral weight from the free carriers is captured, $\omega \simeq 1000$ cm^{-1}, resulting in $1/\tau_{op} \simeq 80$ cm^{-1}, which is in excellent agreement with the Drude estimates for the optical scattering rate at low temperature.

C. Electronic structure

Several first-principle calculations have been undertaken to study the electronic [10–13] and vibrational [27,28] properties of $PdCoO_2$; however, we are unaware of any that have dealt with the optical properties. Accordingly, the electronic properties have been calculated using density functional theory (DFT) with the generalized gradient approximation (GGA) using the full-potential linearized augmented plane-wave (FP-LAPW) method [29] with local-orbital extensions [30] in the WIEN2k implementation [31]. The total energy and residual forces have been minimized with respect to the unit cell parameters and the fractional coordinates, respectively (details are provided in the Supplemental Material [32]). The real part of the optical conductivity including the effects of spin-orbit coupling has been calculated from the imaginary part of the

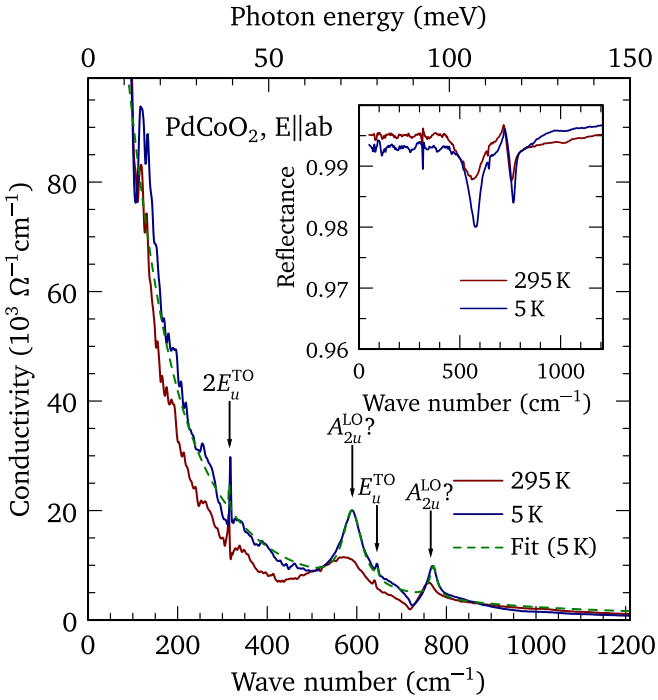

FIG. 5. The real part of the optical conductivity of $PdCoO_2$ for light polarized in the a-b planes at 295 and 5 K in the low-frequency region showing several strong features superimposed on the free-carrier response. The dashed line is the Drude-Lorentz fit to the data at 5 K. Inset: The reflectance at 295 and 5 K over the same frequency interval.

dielectric function, $\sigma_{x,x} = 2\pi\omega \operatorname{Im}\epsilon_{x,x}/Z_0$ [33], using a fine k-point mesh (10 000 k points). The calculated conductivity due to interband transitions along the a axis ($\sigma_{x,x}$) shown in Fig. 2 is in excellent agreement with the experimental results. The intraband plasma frequencies have also been calculated for the a and c axes with values of $\omega_{p,a} \simeq 31\,500$ cm^{-1} and $\omega_{p,c} \simeq 3660$ cm^{-1}, respectively, indicating a large anisotropy in the effective mass $\omega_{p,a}^2/\omega_{p,c}^2 = m_c^*/m_a^* \simeq 74$; this is consistent with the quasi-2D nature of this material. The value for $\omega_{p,a}$ is in good agreement with the experimentally determined average in-plane value of $\omega_p \simeq 33\,300$ cm^{-1}.

D. Vibrational properties

The low-frequency optical conductivity in Fig. 2 has some structure superimposed on the free-carrier response. The optical conductivity at 295 and 5 K is shown in Fig. 5 below ~0.15 eV; several very strong features are observed, which are also present in the reflectance (shown in the inset). The irreducible vibrational representation for $PdCoO_2$ for the $R\bar{3}m$ space group is $\Gamma_{\text{vib}} = A_{1g} + E_g + 2A_{2u} + 2E_u$; the A_{1g} and E_g modes are Raman active, while the A_{2u} and E_u modes are infrared active along the c and a axes, respectively [23]. While only two infrared-active vibrations are expected for light polarized in the a-b planes, it is clear from Fig. 5 that there are at least four modes present. The features in the optical conductivity have been fit to Lorentzian oscillators [Eq. (1)], and the results shown in Table III.

TABLE III. The fitted Lorentz oscillator parameters are listed for the four features observed in $\sigma_1(\omega)$ at 5 K in Fig. 5, and compared with the calculated frequencies and atomic intensities of $PdCoO_2$ for the infrared-active modes at the zone center. All units are in cm^{-1} unless otherwise indicated.

		Experiment (5 K)			Theory[a]			
Mode	(Branch)	ω_i	γ_i	Ω_i	ω_{calc}	Pd	Co	O
$E_{u,1}$	(TO)	–	–	–	154	0.45	0.43	0.12
A_{2u}	(TO)	–	–	–	287	0.43	0.52	0.05
$2E_{u,1}$	(TO)	318	2.3	1334	308	–	–	–
A_{2u}?	(LO)	588	53	6566	–	–	–	–
$E_{u,2}$	(TO)	645	6.7	872	628	0.00	0.28	0.72
A_{2u}	(TO)	–	–	–	661	0.03	0.18	0.79
A_{2u}?	(LO)	764	13.5	2080	–	–	–	–

[a]This work.

There are several existing first-principles calculations of the lattice modes in this material [27,28], which we have reproduced using the frozen-phonon (direct) method to determine the atomic character of the zone-center TO vibrations [34] (details are provided in the Supplemental Material); the results are summarized in Table III. The low-frequency E_u mode involves mainly the Pd and Co atoms and is calculated to be at ≃154 cm^{-1}; this mode is not observed due to the extremely large electronic background. However, there is a sharp feature at 318 cm^{-1} that is tentatively assigned as the second harmonic of this vibration. The high-frequency E_u mode, which involves the Co and O atoms, is calculated to be at ≃628 cm^{-1} and is observed at 645 cm^{-1}. Although this feature appears relatively insignificant, it possesses significant oscillator strength (Table III); it only appears weak because it is superimposed on a large electronic background. The two strong features at ≃588 and 764 cm^{-1} fall into the characteristic energy range expected for lattice vibrations; however, they do not correspond to any of the calculated infrared or Raman vibrations. Both modes, the one at 588 cm^{-1} in particular, narrow considerably and harden at low temperature, ruling out artifacts from absorptions elsewhere in the optical path as their origin. These structures are considerably broader and stronger than expected for infrared-active vibrations. It appears these features are manifestations of the c-axis A_{2u} LO modes, which have been observed in the cuprates and have the same antiresonant line shape in the reflectance [16] (inset of Fig. 5). For a single oscillator, $\Omega_0^2 = \epsilon_\infty(\omega_{\text{LO}}^2 - \omega_{\text{TO}}^2)$. Using the values in Table III and $\epsilon_\infty \simeq 3.4$ returned from the fits, A_{2u} LO modes at the correct positions can be obtained using $\Omega_0 \simeq$ 700–950 cm^{-1}. This suggests the presence of electron-phonon coupling where the out-of-plane displacements of the Pd and O atoms allow the in-plane carriers to couple of the long-range electric field [16].

IV. CONCLUSIONS

The in-plane optical properties of $PdCoO_2$ reveal that the free-carrier intraband response falls well below the interband transitions, allowing the plasma frequency to be determined from the f-sum rule; the value of $\omega_p \simeq 33\,300$ cm^{-1} is in good agreement with fits to the Drude-Lorentz model, as well

as first-principle calculations. While the optically determined scattering rate at room temperature of $1/\tau_{\rm op} \simeq 100$ cm^{-1} is in good agreement with transport measurements, it displays little temperature dependence, and at low temperature $1/\tau_{\rm op} \gg 1/\tau_{\rm tr}$. This inconsistency is resolved by assuming Fermi liquid behavior where the scattering rate varies quadratically with both temperature and frequency; $1/\tau_{\rm op}$ is then the average of $1/\tau(\omega) \propto \omega^2$ over the region of the free-carrier response, unlike the $1/\tau(\omega) \propto \omega$ behavior observed in the cuprates. Despite the high conductivity of this material, at least one in-plane infrared-active E_u mode is identified. The two additional features appear to be manifestations of the A_{2u} c-axis LO modes coupling to the in-plane carriers; the strength and width of these features suggests that electron-phonon coupling is present.

ACKNOWLEDGMENTS

We would like to acknowledge helpful conversations with A. Akrap and J. Hwang. Work at Brookhaven National Laboratory was supported by the Office of Science, U.S. Department of Energy under Contract No. DE-SC0012704.

[1] R. D. Shannon, D. B. Rogers, and C. T. Prewitt, Chemistry of noble metal oxides. I. Syntheses and properties of ABO2 delafossite compounds, Inorg. Chem. **10**, 713 (1971).

[2] M. Tanaka, M. Hasegawa, and H. Takei, Growth and anisotropic physical properties of $PdCoO_2$ single crystals, J. Phys. Soc. Jpn. **65**, 3973 (1996).

[3] C. W. Hicks, A. S. Gibbs, A. P. Mackenzie, H. Takatsu, Y. Maeno, and E. A. Yelland, Quantum Oscillations and High Carrier Mobility in the Delafossite $PdCoO_2$, Phys. Rev. Lett. **109**, 116401 (2012).

[4] P. J. W. Moll, P. Kushwaha, N. Nandi, B. Schmidt, and A. P. Mackenzie, Evidence for hydrodynamic electron flow in $PdCoO_2$, Science **351**, 1061 (2016).

[5] J. Zaanen, Electrons go with the flow in exotic material systems, Science **351**, 1026 (2016).

[6] V. J. Emery and S. A. Kivelson, Superconductivity in Bad Metals, Phys. Rev. Lett. **74**, 3253 (1995).

[7] N. E. Hussey, K. Takenaka, and H. Takagi, Universality of the Mott-Ioffe-Regel limit in metals, Philos. Mag. **84**, 2847 (2004).

[8] The Mott-Ioffe-Regel limit is the point at which the mean free path is equal to a lattice spacing and the Boltzmann description of diffusive transport breaks down.

[9] D. N. Basov and T. Timusk, Electrodynamics of high-T_c superconductors, Rev. Mod. Phys. **77**, 721 (2005).

[10] R. Seshadri, C. Felser, K. Thieme, and W. Tremel, Metal-metal bonding and metallic behavior in some ABO_2 delafossites, Chem. Mater. **10**, 2189 (1998).

[11] V. Eyert, R. Frésard, and A. Maignan, On the metallic conductivity of the delafossites $PdCoO_2$ and $PtCoO_2$, Chem. Mater. **20**, 2370 (2008).

[12] K. Kim, H. C. Choi, and B. I. Min, Fermi surface and surface electronic structure of delafossite $PdCoO_2$, Phys. Rev. B **80**, 035116 (2009).

[13] K. P. Ong, J. Zhang, J. S. Tse, and P. Wu, Origin of anisotropy and metallic behavior in delafossite $PdCoO_2$, Phys. Rev. B **81**, 115120 (2010).

[14] H.-J. Noh, J. Jeong, J. Jeong, E.-J. Cho, S. B. Kim, K. Kim, B. I. Min, and H.-D. Kim, Anisotropic Electric Conductivity of Delafossite $PdCoO_2$ Studied by Angle-Resolved Photoemission Spectroscopy, Phys. Rev. Lett. **102**, 256404 (2009).

[15] A. P. Mackenzie, The properties of ultrapure delafossite metals, Rep. Prog. Phys. **80**, 032501 (2017).

[16] M. Reedyk and T. Timusk, Evidence for A-B-Plane Coupling to Longitudinal c-Axis Phonons in High-T_c Superconductors, Phys. Rev. Lett. **69**, 2705 (1992).

[17] H. Takatsu, S. Yonezawa, S. Fujimoto, and Y. Maeno, Unconventional Anomalous Hall Effect in the Metallic Triangular-Lattice Magnet $PdCrO_2$, Phys. Rev. Lett. **105**, 137201 (2010).

[18] C. C. Homes, M. Reedyk, D. A. Crandles, and T. Timusk, Technique for measuring the reflectance of irregular, submillimeter-sized samples, Appl. Opt. **32**, 2976 (1993).

[19] M. Dressel and G. Grüner, *Electrodynamics of Solids* (Cambridge University Press, Cambridge, 2001).

[20] F. Wooten, *Optical Properties of Solids* (Academic, New York, 1972), pp. 244–250.

[21] D. W. Lynch and W. R. Hunter, Comments on the optical constants of metals and an introduction to the data for several metals, in *Handbook of Optical Constants of Solids*, edited by E. D. Palik (Academic, Boston, 1985), pp. 275–367.

[22] K. Momma and F. Izumi, *VESTA3* for three-dimensional visualization of crystal, volumetric and morphology data, J. Appl. Crystallogr. **44**, 1272 (2011).

[23] H. Takatsu, S. Yonezawa, S. Mouri, S. Nakatsuji, K. Tanaka, and Y. Maeno, Roles of high-frequency optical phonons in the physical properties of the conductive delafossite $PdCoO_2$, J. Phys. Soc. Jpn. **76**, 104701 (2007).

[24] S. V. Dordevic and D. N. Basov, Electrodynamics of correlated electron matter, Ann. Phys. **15**, 545 (2006).

[25] C. C. Homes, Y. M. Dai, J. S. Wen, Z. J. Xu, and G. D. Gu, $FeTe_{0.55}Se_{0.45}$: A multiband superconductor in the clean and dirty limit, Phys. Rev. B **91**, 144503 (2015).

[26] A useful conversion is 1 eV = 8065.5 cm^{-1}.

[27] S. Kumar, H. C. Gupta, and Karandeep, First principles study of structural, bonding and vibrational properties of $PtCoO_2$, $PdCoO_2$ and $PdRhO_2$ metallic delafossites, J. Phys. Chem. Solids **74**, 305 (2013).

[28] L. Cheng, Q.-B. Yan, and M. Hu, The role of phonon-phonon and electron-phonon scattering in thermal transport in $PdCoO_2$, Phys. Chem. Chem. Phys. **19**, 21714 (2017).

[29] D. J. Singh, *Planewaves, Pseudopotentials and the LAPW Method* (Kluwer Academic, Boston, 1994).

[30] D. Singh, Ground-state properties of lanthanum: Treatment of extended-core states, Phys. Rev. B **43**, 6388 (1991).

[31] P. Blaha, K. Schwarz, G. K. H. Madsen, D. Kvasnicka, and J. Luitz, WIEN2k, *An Augmented Plane Wave Plus Local Orbitals Program for Calculating Crystal Properties* (Techn. Universität Wien, Austria, 2001).

[32] See Supplemental Material at http://link.aps.org/supplemental/10.1103/PhysRevB.99.195127 for details of electronic structure calculations and lattice dynamics.

[33] C. Ambrosch-Draxl and J. O. Sofo, Linear optical properties of solids within the full-potential linearized augmented planewave method, Comput. Phys. Commun. **175**, 1 (2006).

[34] K. Parlinksi, Software PHONON (2003).